analytical chemistry

Article

pubs.acs.org/ac

Depth Profiling Nano-Analysis of Chemical Environments using Resonant Raman Spectroscopy at Grazing Incidence Conditions

Juan José Leani,*[,†] Héctor J. Sánchez,[†,‡] Roberto D. Pérez,[†,‡] and Carlos Pérez[§]

[†]Facultad de Matemática Astronomía y Física, Universidad Nacional de Córdoba, 5000 Córdoba, Argentina

[‡]Consejo Nacional de Investigaciones Científicas y Técnicas (CONICET), C1033AAJ Buenos Aires, Argentina

[§]Laboratorio Nacional de Luz Síncrotron, CP 6192/CEP 13084-971, Campinas, Brazil

ABSTRACT: Both X-ray total reflection and X-ray Raman scattering techniques were combined to discriminate chemical environments in depth-profiling studies using an energy dispersive system. This allowed, for the first time, to resolve oxidation state on surface nanolayers with a low-resolution system. Samples of pure Cu and Fe oxidized in tap water and salty water, respectively, were studied in the Brazilian synchrotron facility using monochromatic radiation and an EDS setup. The measurements were carried out in total reflection geometry with incident energy lower and close to the K absorption edge of both elements. The results allowed observing the presence of very thin oxide layers, usually not observable with conventional geometries of irradiation. They also permit the identification of the compound present in a particular depth of the sample with nanometric, or even subnanometric, resolution using a low-resolution system.

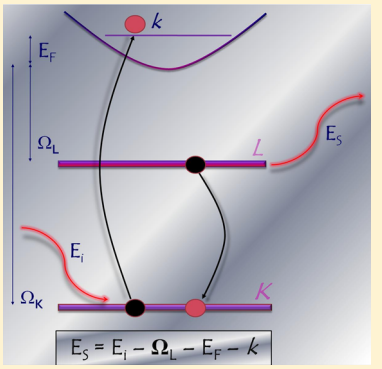

Total reflection of X-rays is a photon effect that gives place to many spectrometric techniques, allowing the study of material surfaces.[1−3] Since the pioneer work of Parrat[1] in 1954 for surface studies of solids by the analysis of the reflected X-ray intensity, many works have been published showing the potentiality of this phenomenon combined with other techniques, such as X-Ray Fluorescence (XRF) in a variety of samples,[4−7] Extended X-ray Absorption Fine Structure (EXAFS)[8,9], and even Inelastic X-ray Scattering (IXS) at grazing incidence conditions was achieved[10,11] at several studied energies. Generally, in order to obtain chemical environment information, these techniques probe edge structure characteristics by tuning the incident energy toward the edge.

As the refractive index is less than unity, X-rays are totally reflected if the glancing angle is less than the critical angle derived from the Snell's law.[3] Even when X-rays are totally reflected, an evanescent wave penetrates the first atomic layers of the surface.[12] Making use of this effect, different depths of a sample surface can be studied by means of scanning the glancing angle of the incident X-ray beam around the critical angle of total reflection. In this way, analysis of the reflected intensity, or the fluorescent emission of the surface, provides a method for studying surface properties, such as variations of electron density with depth (e.g., corrosion, porosity, aging, etc.) with a resolution from Ångströms to hundred nanometers deep.[1]

X-ray Resonant Raman Scattering (RRS) is an inelastic scattering process which presents primary differences compared to other interactions between X-rays and matter; when the energy of the incident photon approaches from below to an absorption edge of the target atom, a strong resonant behavior takes place.[13,14]

In accordance with the absorption−emission model, the RRS process can be represented by the following three steps.[15] (1) The initial state consists of an incident photon with an energy below the K (or L_3, L_2, etc.) absorption edge. (2) The intermediate state. A hole is produced in the K (or L_3, L_2, etc.) shell, and the electron is excited to an unoccupied state; an electron from a higher shell fills the vacancy and a photon is emitted. (3) The final state consists of a hole in the higher shell, a scattered photon and an excited electron (in the continuum or in an unoccupied bound state).

In our case, the incident photon has energy below the K absorption edge, and the K hole is filled by an electron from the L shell. The incident photon has an energy E_i lower than the energy of the K threshold; the energy of the incident photon is absorbed by a K shell electron producing a vacancy and an electron in the continuum with kinetic energy, κ. The K shell hole is filled by an electron from the L shell (being Ω_L, the energy of the L threshold), and a photon is emitted with energy, E_S. This is an example of a KL-type scattering.

If the incident photon has a defined energy, the energy conservation for the scattering process leads to[16]

$$E_i - \Omega_L - E_F = E_S + \kappa \quad (1)$$

where E_F is the Fermi energy.

Unlike fluorescent processes where the emitted photon has a fixed energy and the outgoing electron has the rest of the

Received: January 4, 2013
Accepted: June 19, 2013

   dx.doi.org/10.1021/ac4000317 | *Anal. Chem.* XXXX, XXX, XXX−XXX

available energy, the conservation of energy for this scattering process indicates that between the initial and final states, the available energy has to be shared between the outgoing electron and the emitted photon (i.e., for an incident photon energy, a variety of emitted photon energies are possible).

In the past few years, inelastic X-ray scattering experiments have become a powerful tool for investigating electronic excitations and electronic ground-state properties of many-electron systems. In particular, there is an increasing interest in employing this technique using incident monochromatic radiation at fixed energy (i.e., without the need of an incident energy scan) in combination with high-resolution systems to obtain local structure information, similar to the one obtained with X-ray Absorption Near Edge Structure (XANES) spectroscopy.[17−20] This resonant inelastic X-ray spectroscopy makes use of the fact that in the resonant regime the natural width introduced for the finite lifetime of the 1s hole is removed, allowing a more detail structural discrimination.[21] In this respect, detailed information about pre-edge structures in metals, as relevant information about 1s−3d(4p) transitions, could be obtained by this method. On the other hand, the studied ranges were always situated close (tens of eV) from the energy for the 1s−3d transitions, using very high-resolution spectrometers, since it is not possible to collect correctly the long low-energy tail of Raman peaks using conventional high-resolution systems. This fact has limited, until now, the use of this technique to collect only XANES-like information (from discrete atomic transitions). This work shows the possibility to obtain EXAFS-like information (from interatomic interference processes), using an EDS low-energy system, allowing also depth-resolved discriminations.

Foils of pure Cu and Fe oxidized in tap water and salty water, respectively, were studied at the Brazilian synchrotron facility. The measurements were carried out in total reflection geometry scanning the incident radiation angle around the critical angle with the incident energy lower and close to the K absorption edge of both elements in order to study the RRS emissions.

The RRS spectra were analyzed with dedicated programs for fitting the experimental data to a theoretical expression. Then, residuals were determined in the low-energy side of the RRS peaks. These residuals were treated with a FFT smoothing process, taking into account the instrument function of the detecting system. The residuals show an oscillation pattern that changes smoothly with the incident angle (i.e., with the observed depth) allowing a depth study of the oxidation state with nanometric, and even subnanometric, resolution.

The results show, for the first time, the possibility to obtain detailed structural information by means of resonant Raman scattering in total reflection geometry using a low-resolution system.

■ MEASUREMENTS AND DATA PROCESSING

The measurements were carried out in the XRF station of the D09BXRF beamline[22] at the Brazilian synchrotron facility (LNLS, Campinas).[23] The XRF beamline is equipped with a double-crystal monochromator (≈3 eV at 10 keV). For the measurements performed in this work, the incident beam was collimated with orthogonal slits to 0.5 × 1 mm and monitored with ionization chambers, resulting in a flux on the sample of ~10^8 ph s^{-1} at 10 keV. The detector used in this work was a KETEK AXAS-A solid-state detector with a Be windows of 8 μm and an energy resolution of 139 eV for the Mn Kα line.

The samples consisted of pure Fe and Cu foils (>99.99%) with a thickness of 0.1 mm. The foils were irradiated with monochromatic photons of 7082 eV in the case of Fe and 8929 eV for the Cu sample (i.e., tens of eV below the K absorption edge of these elements in order to inspect the Raman emissions). Although at incident energies far away from the absorption edge, the RRS cross sections significantly decrease,[14] an incident energy closer to the threshold value causes the shape of the RRS peak approaches to the thin fluorescence line,[13] where the studied oscillations could be observed only with the use of very high-resolution spectrometers.

Regarding the oxidation processes, Cu foil was immersed in tap water for 82 h, while Fe foil was immersed in a solution of ~70 cm^3 pure water with ~5 g sodium chloride (common salt) for 58 h. A scanning of the incident radiation angle was performed in both samples.

The depth, with respect to the sample surface, at which the intensity of the incident radiation is reduced to 1/e, is,[1]

$$z_{1/e} = \frac{\lambda}{4\pi B} \quad (2)$$

where λ is the wavelength of the photon and B is given by

$$B = \frac{1}{\sqrt{2}}\sqrt{[(\varphi^2 - \varphi_c^2)^2 + 4\beta^2]^{1/2} - (\varphi^2 - \varphi_c^2)}$$

where φ is the incident radiation angle, φ_c the critical angle for the media, $\beta = \mu\lambda/4\pi$ the imaginary part of the refractive index, and μ the linear absorption coefficient.

The critical angle φ_c could be represented as[3]

$$\varphi_c = \sqrt{2\delta} \quad (3)$$

which is derived from Snell's law. δ is the real part of the refractive index and it is given by

$$\delta = \frac{ne^2\lambda^2}{2\pi mc^2}$$

n is the total number of dispersive electrons per unit volume of the material: $n = N(Z/A)\rho$, where N is Avogadro's number, Z the atomic number, A the atomic weight, and ρ the sample density.

In general, every surface presents some degree of roughness. Surface roughness produces both diffuse scattering and transmission into the reflector. The effect of the surface roughness is to steepen the falloff with the angle of the total reflection curve and to diverge the beam slightly from its specularly reflected direction.[24] In this work, transmission is very low due to the glancing incidence condition; the effects of roughness are reduced and can be neglected.

Figure 1 shows the calculated penetration depth (eq 2) as a function of the incident radiation angle for pure Fe and Fe_2O_3 (incident radiation energy of 7082 eV) and pure Cu and CuO samples (incident radiation energy of 8929 eV). As can be seen, the observed depth just increases ~3.2 Å when the incident angle goes from 0.01° to 0.25°. Thus, the fact that the reflected intensity changes very smoothly with the incident radiation angle far away from the critical angle can be used to reach a very detailed study of the most external layers of a sample.

Oxidation of a surface results in an attenuated electron density if the oxide forms a skin layer on the general surface plane. It is a fact that the rust present in a metal has a volume higher than the volume of the originating mass of the sample.

dx.doi.org/10.1021/ac4000317 | Anal. Chem. XXXX, XXX, XXX−XXX

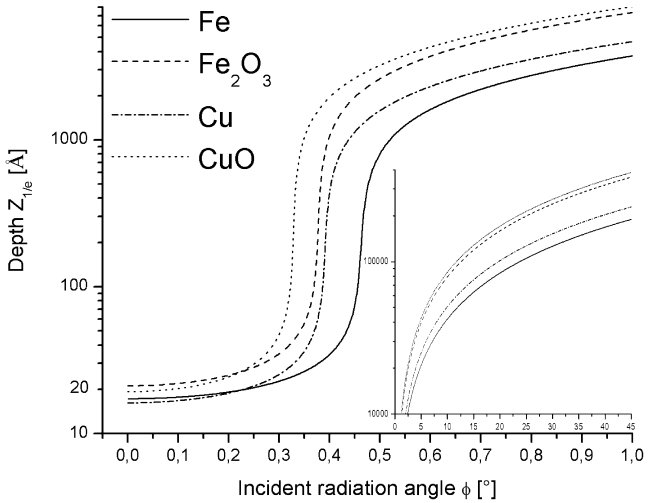

Figure 1. Calculated depth (eq 2) as a function of the incident radiation angle for Fe, Fe_2O_3, Cu, and CuO samples.

In this way, the calculated penetration depth is just an approximation. The electron density reduction respective of a nonoxidized surface induces a discrepancy in the calculated δ value, with this discrepancy carried to the $z_{1/e}$ value. In order to reach an estimation of a more realistic observed depth, we considered a three-layer oxidation distribution. In the case of the Fe foil, we considered the most external layer (from 0 to 100 nm) totally oxidized as Fe(III) (Fe_2O_3), the layer from 100 to 400 nm partially (50%) oxidized, and the deeper layer not oxidized (pure Fe). In the case of the Cu sample, we considered the most external layer (from 0 to 200 nm) completely oxidized as Cu(II) (CuO), the layer from 200 to 850 nm partially (50%) oxidized, and the deeper layer not oxidized (pure Cu). In addition, loose packing, porosity, and other nonuniform electron reduction effects could cause the penetration to be somewhat greater than the calculated value, making these effects very difficult to take into account and quantify. In addition, (see below) the samples show a gradual transition between the oxidized region and the pure bulk, making a correct electron density estimation with the depth unviable. These considerations do not represent a problem for our survey. The aim of this work is to show the potentiality of resonant Raman spectroscopy in the total reflection regime as a tool to study how oxidation states changes with the depth, making the estimated values good enough for our purposes.

Another point to be considered is the contribution to the emitted beam of the radiation produced at upper points in the sample. The contribution of the upper layers is, somehow, present in the emissions of the deeper layers. Nevertheless, the information obtained from the different spectra as a function of the depth clearly shows the variation with the position regarding the oxidation state. The individualization of any contribution from each spectrum is a very complicated task that exceeds the scope of this single paper.

The incident radiation angles (and the corresponding approximated observed depth), respective to the sample surface, were φ = 0.01° (2.11 nm), 0.05° (2.13 nm), 0.1° (2.19 nm), 0.15° (2.30 nm), 0.25° (2.82 nm), 0.56° (231.20 nm), 1.12° (429.20 nm), and 2.12° (870.40 nm) in the case of the Fe foil and φ = 0.8° (488.85 nm), 0.9° (563.85 nm), 1° (637.25 nm), 1.1° (709.59 nm), 1.2° (781.18 nm), 1.3° (852.17 nm), and 45° (22840 nm) for the Cu sample. The values of μ were taken from Hubbell and Seltzer,[25] and ρ data were extracted from Lide.[26] The measuring lifetime for each incident radiation angle were 3000 and 2000 s for Fe and Cu foils, respectively.

Spectra were analyzed with specific programs for spectrum analysis.[27,28] The data fitting of the low-energy side of the Raman peaks was achieved by means of a Lorentzian expression:

$$y = y_0 + \frac{2A}{\pi}\frac{\omega}{4(x - x_0)^2 + \omega^2} \quad (4)$$

where y_0 is the baseline offset, A is the area under the curve from the baseline, x_0 is the center of the peak, and ω is the full width of the peak at half-height.

Data-fitting of the first-order peak is not as crucial as it seems. This fitting does not significantly influence the oscillations produced by the second-order effect. In fact, these oscillations are not present in the first-order theoretical curve. In any case, eventual fitting deviations disappear when the spectra are compared. Even so, the best fitting curve was chosen in order to reproduce mathematically the tail of the spectrum from more than 3000 potential candidates, achieving a regression coefficient $r^2 > 0.999$.

Time-dependent experimental data are frequently contaminated by noise, originated generally from statistics, the experiment itself, or noise related to the measurement process. In this work, a well-known denoising method was employed based on the frequency decomposition of the signal.[29] This method is based on a FFT smoothing procedure, and it was applied with consideration for a Gaussian instrumental function with a σ of 59 eV. The FFT method offers a significant physical sense at the moment of inspecting the experimental data, in opposition to purely mathematical methods (e.g., methods based on pondered averages).

No systematic errors are expected to appear because of the simplicity of the experiment. As each spectrum is obtained at a fixed angle, standing wave effects in the stratified surface are negligible, producing (eventually) small variations in the total intensity but not affecting the Raman oscillation pattern.

With regard to sensitivity, the emission factor corresponding to RRS is essentially the same as the one for X-ray fluorescent lines, and so, sensitivity depends on the sample. The only difference has to do with the different cross sections involved (photoelectric and resonant Raman scattering). In this way, sensitivities for RRS are slightly lower than XRF experiments but follow the same behavior.

With concern for the depth precision, depth is determined by the usual Fresnel theory, which depends on the divergence of the incident beam. In this sense, the depth precision does not depend on the sample, and taking into account that the synchrotron beam presents divergence as low as a μrad, the depth precision reaches a tenth of Angstrom, calculated according to eq 2 for the vertical divergence of the synchrotron beam.

RESULTS AND DISCUSSION

The results in this work do not take into account infrared divergence or bremsstrahlung contributions to the background. Their contributions are important mostly in low energy areas and do not significantly affect the range of the scattered line (i.e., the range of interest of this work).[30] On the other hand, the bremsstrahlung is a smooth and continuous function of the

dx.doi.org/10.1021/ac4000317 | Anal. Chem. XXXX, XXX, XXX−XXX

energy that does not interfere with the fast variations in the spectra that we are studying. Moreover, these effects have the same energy distribution in all the studied samples, being compensated in the spectral comparison.

With regard to self-absorption effects, since both incident and scattered energy are below the absorption edge, absorption is relatively weak and changes are negligible. It also means that the probing volume is almost constant for the whole spectrum, which exempts the need for self-absorption corrections.[31] This low absorption allows a deeper penetration, reaching better depth sample studies. On the other hand, low deposited doses are remarkably useful to investigate X-ray sensitive samples as biological ones.

Corrosion Considerations. Corrosion, or rust, is a natural process that occurs when a material deteriorates due to its interaction with the surrounding environment in which an electrochemical reaction affects the material through oxidation processes.

A water media changes the metal environment into a light form of acid which helps metal rust faster. This acidic transformation occurs with pure water, but when the water is already salty, it starts out as a minor acid environment and becomes an even more powerful electrolyte, facilitating the rusting process. Pure water forms an acidic solution and allows the oxidation process to happen easily; salty water works even better since it is already a catalyst.

The rusting of iron is an electrochemical process that begins with the transfer of electrons from iron to oxygen.[32] The rate of corrosion is affected by water and accelerated by electrolytes, as salt in water. The key reaction is the reduction of oxygen:

$$O_2 + 4e^- + 2H_2O \rightarrow 4OH^-$$

Because it forms hydroxide ions, this process is strongly affected by the presence of acid. Indeed, the corrosion of most metals by oxygen is accelerated at low pH. Providing the electrons for the above reaction is the oxidation of iron that may be described as follows:

$$Fe \rightarrow Fe^{2+} + 2e^-$$

The following redox reaction is crucial for the formation of rust:

$$4Fe^{2+} + O_2 \rightarrow 4Fe^{3+} + 2O^{2-}$$

Additionally, the following multistep acid−base reactions affect the course of rust formation:

$$Fe^{2+} + 2H_2O \leftrightarrow Fe(OH)_2 + 2H^+$$

$$Fe^{3+} + 3H_2O \leftrightarrow Fe(OH)_3 + 3H^+$$

As do the following dehydration equilibria:

$$Fe(OH)_2 \leftrightarrow FeO + H_2O$$

$$Fe(OH)_3 \leftrightarrow FeO(OH) + H_2O$$

$$2FeO(OH) \leftrightarrow Fe_2O_3 + H_2O$$

The iron(II) hydroxide can also be oxidized to form iron(II, III) oxide and molecular hydrogen. This process is described by the Schikorr reaction:

$$3Fe(OH)_2 \leftrightarrow Fe_3O_4 + H_2 + H_2O$$

The crystallized iron(II, III) oxide (Fe_3O_4) is thermodynamically more stable than the iron(II) hydroxide.

From the above equations, it is also seen that the corrosion products are dictated by the availability of water and oxygen. With limited dissolved oxygen, iron(II)-containing materials are favored, including FeO and Fe_3O_4. High oxygen concentrations favor ferric materials with the nominal formulas $Fe(OH)_{3-x}O_{x/2}$. The nature of rust changes with time, sometimes reflecting the slow rates of the reactions of solids.

Furthermore, these complex oxidation processes are affected by the presence of other ions, such as Ca^{2+}, which serves as an electrolyte, and thus accelerates rust formation or combines with the hydroxides and oxides of iron to precipitate on a variety of Ca−Fe−O−OH species.

The accurate identification of iron(II) hydroxide could be relevant, since it has been investigated as an agent for the removal of toxic selenate and selenite ions from water systems such as wetlands. The iron(II) hydroxide reduces these ions to elemental selenium, which is insoluble in water and precipitates out.[33]

Similarly, Cu metal is oxidized for the combination of water and oxygen dissolved in it. This oxidation is an electrochemical process that begins with the transfer of electron from copper to oxygen. Since the possible oxidation states of copper are Cu(I) and Cu(II), in the presence of water there are two possibilities provided below. Oxidations of Cu:

$$Cu \rightarrow Cu^{+2} + 2e^-$$

$$2Cu \rightarrow 2Cu^{+2} + 4e^-$$

Overall reactions in water:

$$Cu \rightarrow CuO + H_2$$

$$2Cu \rightarrow Cu_2O + H_2$$

Cuprous oxide (Cu_2O) has a cubic structure; cupric oxide (CuO) has a monolithic structure. The Cu_2O unit cell contains 4 copper and 2 oxygen atoms, where Cu atoms were arranged in a fcc sublattice and O atoms in a bcc sublattice. In the CuO arrangement, the copper atom is coordinated by four oxygen atoms in an approximately square planar configuration.[34]

As mentioned before, the formation of cupric or cuprous oxides depend on the availability of water, oxygen, and the conditions of the reaction. Underwater and at room temperatures, the most common oxidation state of Cu is Cu(II), being that Cu(I) oxide is more common at higher reaction temperatures. As in the Fe case, these Cu oxidation processes could be affected by the presence of other ions in water, changing the oxidation formation dynamics, or combining with them and precipitating in a variety of Cu species. Furthermore, recently, it has been observed that copper pipes deteriorate under the influence of microorganisms, e.g., *Pseudomonas fluorescence*, *Pseudomonas Aerugenosa*, Nocardia *Azotobacter vinelandii*, *Xanthomonas campestris*, and other uncharacterized strains, including fungi and diatoms, known to be present in surface waters. The mechanisms of these corrosion processes are still unknown.[35] Finally, it is a well-known fact that Cu(I) compounds, in the course of time, degrade to Cu(II) oxide in an air atmosphere.[36]

Clearly, all the effects mentioned in these considerations, some of them of unknown mechanisms, affect the oxidation processes in a nonquantifiable way. In this respect, it is not viable a satisfactory separation, identification, or control of the physical and chemical variables involved in the oxidation processes, reaching in this way a nonideal resulting sample.

dx.doi.org/10.1021/ac4000317 | *Anal. Chem.* XXXX, XXX, XXX−XXX

Figure 2 shows low-energy residuals (just below the Raman peak center and after the smoothing procedure) between the experimental Raman spectra and the data fitting using eq 4, for the Cu sample in conventional geometry (45°−45°) for the three points of measurement: without oxide, in the oxidized part, and in the interface between them. It is evident from Figure 2 that the three spectra are indistinguishable for all practical purposes. This behavior is due to the fact that at this angle, transmission is imposing and characteristic X-rays are produced in the bulk of the material, some micrometers under the surface. The oxide layer present in the sample is very thin due to the oxidation process, being not correctly excited with the use of conventional irradiation geometries (45°−45°).

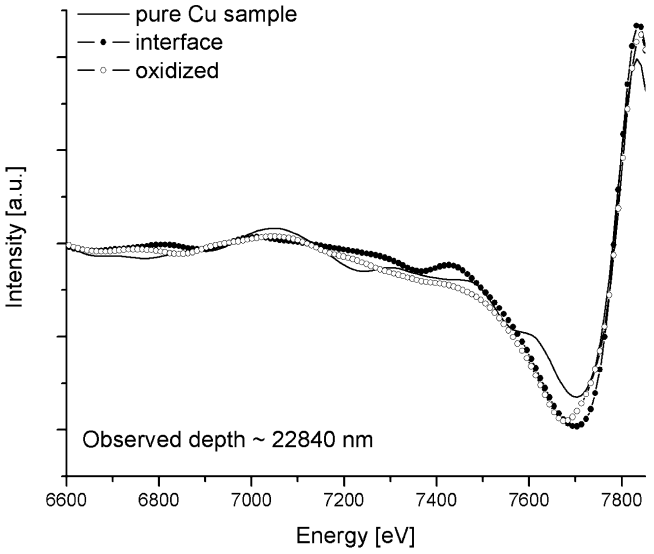

Figure 2. Residuals between the experimental Raman spectra and the data fittings using eq 4 for the Cu sample in conventional geometry (45°−45°) for three point of measurement: without oxide (pure Cu sample), interface and oxidized part.

Figure 3 shows the X-ray Raman spectra for two studied depths (2.82 nm and 870.40 nm) for the Fe foil. Error bars based on the Poisson statistic from the total Raman intensity are given. Upper left inset shows a fit of the X-ray Raman tail. Clearly, in order to obtain chemical information from these spectra, an analysis procedure is needed.

Figures 4 and 5 show the low-energy residuals (just below the Raman peak center and after the smoothing procedure)

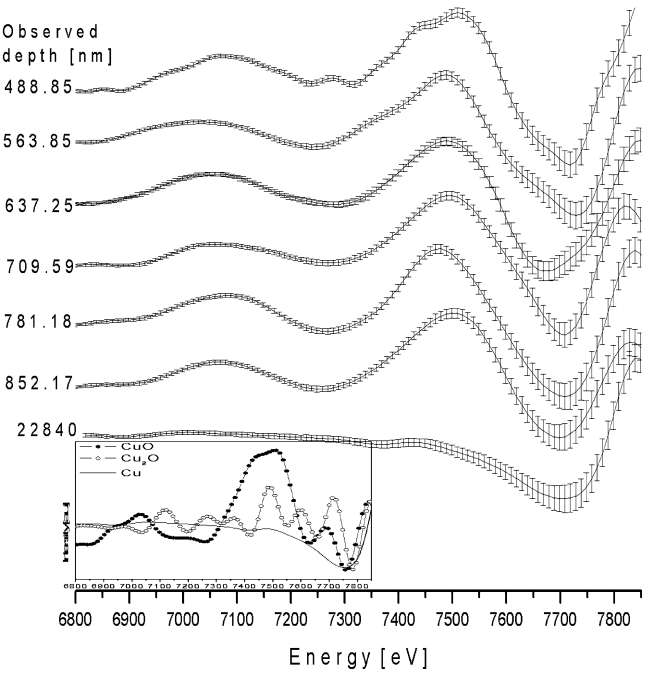

Figure 4. Residuals between the experimental Raman spectra and the Lorentzian fitting for the oxidized Cu sample as a function of depth. Error bars are given. Inset: Cu, Cu_2O, and CuO residuals between experimental Raman spectra and the data fitting, irradiating pure powder compounds in the 45°−45° geometry.[36].

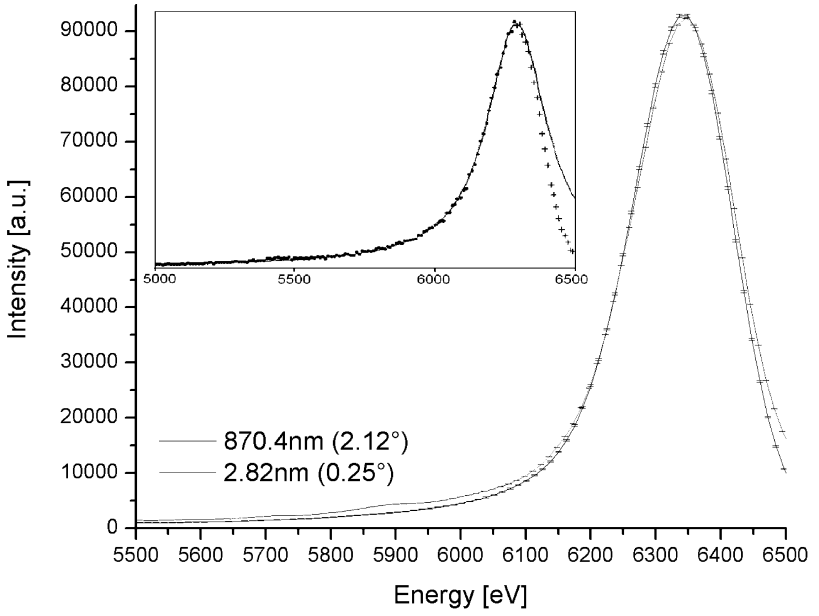

Figure 3. Comparison between X-ray Raman spectra for two studied depths in Fe foil. Error bars are given. Inset: example of Lorentzian fit.

dx.doi.org/10.1021/ac4000317 | Anal. Chem. XXXX, XXX, XXX−XXX

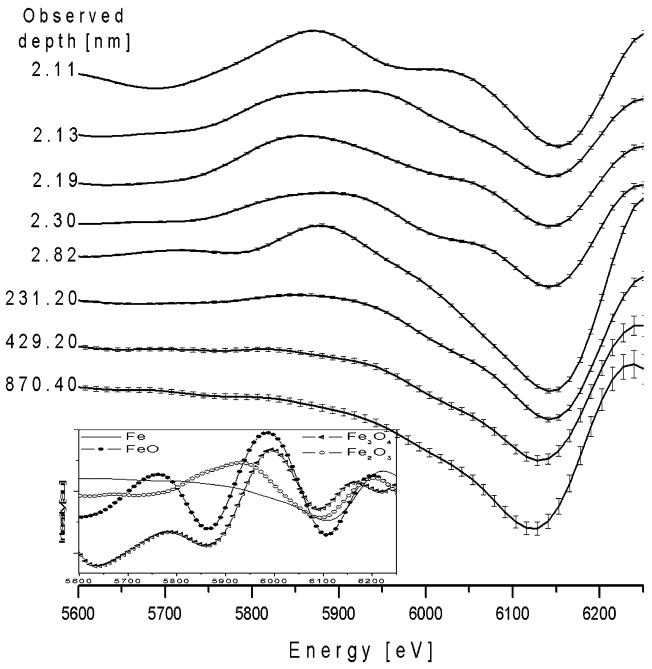

Figure 5. Residuals between the experimental Raman spectra and the Lorentzian fitting for the oxidized Fe foil as a function of depth. Error bars are given. Inset: Fe, FeO, Fe_3O_4, and Fe_2O_3 residuals between the experimental Raman spectra and the data fitting, irradiating pure powder compounds in the 45°−45° geometry[37].

between the experimental Raman spectra and the Lorentzian fitting as a function of the studied depth for the oxidized Cu and Fe foils, respectively. The inset figures show residuals between experimental Raman spectra and data fitting for pure Cu and Fe compounds, respectively, measured from compacted powder in conventional geometry.[37,38] Error bars based on the Poisson statistic from total Raman intensity are given.

If any of the oscillation patterns shown in Figure 4 (see e.g. 637.25 nm) are compared with the one shown in the inset for a Cu(II) compound, in this case CuO, a remarkable similitude between both patterns can be observed (see the region around 7050 and 7500 eV). This result clearly exposes the fact that external layers of the sample are oxidized as a cupric oxide, changing the intensity smoothly with the depth, although keeping this oxidation state, to reach the pure Cu state sufficiently deep.

In the case of the Fe sample, it can be seen from Figure 5 that the oscillation patterns, present in the residuals, change smoothly with the observed depth. The most external layers of the sample (see example 2.11 nm) show strong oscillations at ∼5900 eV and ∼6000 eV. As the incident radiation penetrates into the sample, deeper layers of the foil are revealed (see example 2.82 nm), showing a similar oscillation pattern, this time without the shoulder at ∼6000 eV. As the studied layers are deeper into the sample (see 231.20 nm), the main oscillation at ∼5900 eV becomes less intense, being the corresponding pattern smoother. Finally, when the incident angle is bigger, the observed depth reveals a very smooth pattern lacking of prominent oscillations.

If the oscillation patterns present in the residuals of pure Fe compounds shown in the inset are compared with the patterns shown in Figure 5, relevant information can be obtained. The oscillation patterns belonging to the most superficial layers (see 2.11 nm) seem to be a mixture between the patterns of Fe(III) (Fe_2O_3) and Fe(II, III) (Fe_3O_4), since the most intense peak appears at ∼5900 eV and the shoulder at ∼6000 eV. Deeper layers (2.82 nm) expose patterns very similar to the one of Fe_2O_3, since the shoulder is gone. The Fe(III)-like pattern become smoother as the layers are deeper in the sample, arriving finally to a smooth pattern empty of marked oscillations in the pure Fe bulk (see 870.40 nm).

In summary, the results demonstrate that the pure Cu foil immersed in tap water is oxidized as a Cu(II) (cupric oxide), decreasing gradually the amount of oxidation as the analyzed depth increases. In the case of the Fe foil immersed in salty water, the sample seems to be oxidized mainly as Fe(III) (ferric oxide) decreasing smoothly the amount of oxidation as the observed depth increases, presenting also a thin contribution of Fe(II, III) (ferric ferrous oxide) in the most external layers of the sample. These results have a consistent behavior with the arguments exposed in the corrosion considerations above.

Although these surveys still represent only qualitative results (and considering that the noncontrolled oxidation contributions mentioned before could also be present), the application of this new RRS technique in total reflection geometry not only allowed to observe the presence of very thin oxides, invisible with the use of conventional geometries, but also permitted the identification of the oxidation state present in a particular depth of the sample with nanometric, or even subnanometric, resolution. Moreover, if the surface layers are well-represented as parallel planes to the surface (e.g., stratified media) this technique could provide a precise determination of the width and position of the different oxide layers or layers with different chemical environments of the absorbing atom.

Finally, it should be remarked that these results were obtained using a low-resolution Energy Dispersive System (EDS), allowing measuring times shorter than the typical ones using high resolution devices (i.e., WDS spectrometers). Moreover, back-diffraction geometries, usually used to reach high resolution in WDS systems, do not allow the acquisition of the entire Raman spectrum from transitional metal elements, making this type of analysis unrealizable. Finally, taking into account that RRS is a second-order process, high resolution systems based in two analyzer crystals require an unviably long measuring time in order to obtain spectra with good statistics.

CONCLUSIONS

In this work, both resonant Raman scattering and total reflection techniques are used combined as a hybrid tool allowing for discrimination of oxidation states in surface nanolayers of materials using, for the first time, a low EDS resolution spectrometer. Due to the versatility of emission techniques, several possibilities appear from the combination of RRS spectroscopy with other X-ray techniques, even three-dimensional analysis by RRS combined with confocal setups. This new RRS chemical-environment technique will offer a unique opportunity to study the oxidation state of different kinds of samples, reaching a complete characterization, impossible to achieve by conventional absorption methods.

Currently, further investigations are carried out in order to reach a complete understanding of the involved processes with the aim of turning this novel method into a true and complete analytical tool.

In addition, the evolution of dynamic processes could be studied in detail with time resolution as fine as the frequency of the pulse rate of the source. This particular characteristic is a consequence of the absence of the energy scanning required by

dx.doi.org/10.1021/ac4000317 | Anal. Chem. XXXX, XXX, XXX−XXX

the current conventional techniques like XANES, EXAFS, etc. The only requirement for dynamic studies with RRS is a pulsed monochromatic beam, like the new FELs sources. The potential of this technique combined with its simplicity will allow extremely detailed studies of samples of interest and physical processes that are currently not feasible.

AUTHOR INFORMATION

Corresponding Author

*E-mail: lj@famaf.unc.edu.ar.

Notes

The authors declare no competing financial interest.

ACKNOWLEDGMENTS

This work was partially supported by the LNLS (Campinas, Brazil).

REFERENCES

(1) Parrat, L. G. *Phys. Rev.* **1954**, *95*, 359.
(2) Tolan, M. *X-Ray Scattering from Soft-Matter Thin Films*; Springer: N.Y., 1999.
(3) Koch, E.E., *Handbook on Synchrotron Radiation 1A*, North-Holland Publishing Company: Amsterdam, 1983.
(4) Iida, A.; Yoshinaga, A.; Sakurai, K.; Gohshi, Y. *Anal. Chem.* **1986**, *58*, 394.
(5) Vázquez, C.; Boeykens, S.; Elkin, D. *Technical Briefs in Historical Archaeology* **2010**, *5*, 10.
(6) Prange, A. *Spectromchim. Acta, Part B* **1989**, *44*, 437.
(7) Klockenkāmper, R.; von Bohlen., A. *J. Anal. At. Spectrom.* **1992**, *7*, 273.
(8) Barchewitz, R.; Cremonese-Visicato, M.; Onori, G. *J. Phys. C: Solid State Phys.* **1978**, *11*, 4439.
(9) Barrett, N. T.; Gibson, P. N.; Greaves, G. N.; Mackle, P.; Roberts, K. J.; Sacchi, M. *J. Phys. D: Appl. Phys.* **1989**, *22*, 542.
(10) Murphy, B. M.; Müller, M.; Stettner, J.; Requardt, H.; Serrano, J.; Krisch, M.; Press, W. *J. Phys.: Condens. Matter* **2008**, *20*, 224001.
(11) Fister, T. T.; Fong, D. D.; Eastman, J. A.; Iddir, H.; Zapol, P.; Fuoss, P. H. *Phys. Rev. Lett.* **2011**, *106*, 037401.
(12) Born, M.; Wolf, E. *Principles of Optics*; Pergamon Press: Oxford, 1980.
(13) Eisemberger, P.; Platzman, P. M.; Winick, H. *Phys. Rev. Lett.* **1976**, *36*, 623.
(14) Kotani, A.; Shin, S. *Rev. Mod. Phys.* **2001**, *73*, 201.
(15) Sánchez, H. J.; Valentinuzzi, M. C.; Pérez, C. *J. Phys. B: At., Mol. Opt. Phys.* **2006**, *39*, 4317.
(16) Rubensson, J. *J. Electron Spectrosc. Relat. Phenom.* **2000**, *135*, 110−111.
(17) Szlachetko, J.; Dousse, J.-Cl; Berset, M.; Fennane, K.; Szlachetko, M. *Phys. Rev. A* **2007**, *75*, 022512.
(18) Hayashi, H. *Anal. Sci.* **2008**, *24*, 15.
(19) Dräger, G.; Machek, P. *Phys. Rev. B* **2009**, *79*, 033103.
(20) Hayashi, H. *X-Ray Spectrom.* **2011**, *40*, 24.
(21) Hämäläinen, K.; Siddons, D. P.; Hastings, J. B.; Berman, L. E. *Phys. Rev. Lett.* **1991**, *67*, 2850.
(22) Pérez, C. A.; Radke, M.; Sánchez, H. J.; Tolentino, H.; Neuenshwander, R. T.; Barg, W.; Rubio, M.; Silveira Bueno, M. I.; Raimundo, I. M.; Rohwedder, J. R. *X-Ray Spectrom.* **1999**, *28*, 320.
(23) Rodrigues, A. R. D.; Farias, R. H. A.; Ferreira, M. J.; Franco, G. S.; Janhnel, L. C.; Lin, L.; Lira, A. C.; Neuneschwander, R. T.; Pardine, C.; Rafael, F.; Rosa, A.; Scorzato, C.; Goncalves da Silva, C. E. T., Romeu da Silva, A.; Tavares, P. F.; Wisnivesky, D.; Craievich, A. In *Commissioning and Operation of the Brazilian Synchrotron Light Source*, Proceedings of the Particle Accelarator Conference—PAC97, Vancouver, Canada May 12−16, 1997; Comyn, M.; Craddock, M. K.; Reiser, M.; Thomson, J., Eds.; IEEE: Piscataway, NJ, 1998.
(24) Kimball, J. C.; Bittel, D. J. *J. Appl. Phys.* **1993**, *74*, 877.
(25) Hubbell, J. H.; Seltzer, S. M. *Tables of X-Ray Mass Absorption Coefficients and Mass Energy*; NISTIR 5632, NIST: Gaithersburg, Maryland, 1995.
(26) *CRC Handbook of Chemistry and Physics*, 80th ed.; Lide, D.R., Ed.; CRC Press: Boca Raton, Florida, 1999.
(27) *PeakFit*, version 4.12 for Windows; SeaSolve Software, Inc.: San Jose, CA, 2003 (portions from SYSTAT Software Inc.: Chicago, 2000-2003).
(28) *TableCurve*, version 1.11 for Windows; AISN Software, Inc.: Florence, Oregon, 1993.
(29) Zhang, Q.; Aliaga-Rossel, R.; Choi, P. *Meas. Sci. Technol.* **2006**, *17*, 731.
(30) Bannett, Y.; Rapaport, D.; Freund, I. *Phys. Rev. A.* **2011**, *16*, 1977.
(31) Hayashi, H.; Udagawa, Y.; Caliebe, W. A.; Kao, C.-C. *Chem. Phys. Lett.* **2003**, *371*, 125.
(32) Gräfen, H.; Horn, E.; Schlecker, H.; Schindler, H. Corrosion. In *Ullmanńs Encyclopedia of Industrial Chemistry*; Wiley-VCH: Weinheim, Germany, 2000.
(33) Zingaro, R. A.; Dufner, D. C.; Murphy, A. P.; Moody, C. D. *Environ. Int.* **1997**, *23*, 299.
(34) Forsyth, J. B.; Hull, S. *J. Phys.: Condens. Matter* **1991**, *3*, 5257.
(35) Paradies, H. H.; Thies, M.; Hinze, U. *Rigaku J.* **1996**, *13*, 16.
(36) Greenwood, N. N.; Earnshaw, A. *Chemistry of the Elements*, 2nd ed.; Butterworth-Heinemann, 1997.
(37) Leani, J. J.; Sánchez, H. J.; Valentinuzzi, M. C.; Pérez., C. *J. Anal. At. Spectrom.* **2011**, *26*, 378.
(38) Leani, J. J.; Sánchez, H. J.; Valentinuzzi, M. C.; Pérez, C. *X-Ray Spectrom.* **2011**, *40*, 254.